

Synthesis of new rhodium(III) complex by benzylic C—S bond cleavage of thioether containing NNS donor Schiff base ligand: Investigation of catalytic activity towards transfer hydrogenation of ketones

Sujan Biswas, Chandan Kumar Manna, Rahul Naskar, Akash Das, Tapan Kumar Mondal*

Inorganic Chemistry Section, Department of Chemistry, Jadavpur University, Kolkata 700032, India

ARTICLE INFO

Keywords:

Rhodium(III) complex
C—S bond cleavage
Electrochemistry
Transfer hydrogenation of ketones
DFT computation

ABSTRACT

A new rhodium(III)-triphenylphosphine mixed ligand complex, $[\text{Rh}(\text{PPh}_3)(\text{L})\text{Cl}_2]$ (**1**) is synthesized by benzylic C—S bond cleavage of L-CH₂Ph ligand (where, L-CH₂Ph = 2-(benzylthio)-N-(pyridin-2-ylmethylene)aniline). The complex is thoroughly characterized by several spectroscopic techniques. Geometry of the complex is confirmed by single crystal X-ray crystallography. Electronic structure, redox properties, absorption and emission properties of the complex were studied. DFT and TDDFT calculations were carried out to interpret the electronic structure and absorption properties of the complex respectively. The synthesized Rh(III) complex was tested as catalyst towards transfer hydrogenation reaction of ketones in ^tPrOH and an excellent catalytic conversion was observed under mild conditions.

1. Introduction

It is well-known that C—S bonds can be activated by transition metals to form novel sulfur compounds or sulfide complexes [1–3] and this process is extensively studied for the last few decades due to its importance in industry [4–6]. Recently, transition-metal mediated C—S bond activation and cleavage is applied in diverse bioorganic and synthetic chemistry [7,8]. Moreover, transition metals mediated C—S bond activation along with the transformation processes are of stimulating interest from the perspective of synthetic, mechanistic as well as catalytic aspects [9–11]. Transition metal mediated cleavage of both C(aryl)-S and C(alkyl)-S bonds are extensively studied. Hanton et al. reported Cl⁻ triggered facile C(alkyl)-S cleavage of thioether moiety in platinum(II) complex [12]. Goswami et al. reported the effect of reaction temperature and $d\pi(\text{M}) \rightarrow \pi(\text{N}=\text{N})$ on C(alkyl)-S cleavage in platinum(II)-thioether complex [13]. Pramanik et al. explored the C(alkyl)-S cleavage in Rh(III) and Ir(III) complexes in presence of excess PPh₃ [14,15]. In recent years, Biswas et al. reported the activation of both C(aryl)-S and C(alkyl)-S bonds to form cyclometalates and metal-thiolato complexes respectively of group 9 metals [16]. In our previous works, we have reported the synthesis of Pd(II), Ru(II) and Rh(III) complexes by metal induced C(alkyl)-S and C(aryl)-S bond scission of thioether containing ligand systems [17–20]. Herein, we have synthesized a new Rh(III)-

triphenylphosphine complex supported by a tridentate pyridine-imine-thiolato ligand backbone via benzylic C—S bond cleavage of the thioether ligand, L-CH₂Ph (where, L-CH₂Ph = 2-(benzylthio)-N-(pyridin-2-ylmethylene)aniline). It's worth to mention here that the benzylic group plays an important role to cleavage of the C—S bond for the present case. In our previous work, no C—S bond scission was observed and a S(Me)-Rh coordination mode was found under the similar reaction conditions [21].

On the other hand, transfer hydrogenation of ketone to the corresponding alcohol is one of the most important fundamental subjects in modern synthetic chemistry [22,23] and is a convenient method to reduce carbonyl compounds without the use of hazardous hydrogen gas or moisture-sensitive hydride reagents [24–27]. Moreover, the transfer hydrogenation of ketones is widely accepted in industry as a cost-effective way for the production of a number of hydroxylated organic products [28]. Over the last few decades, significant effort on hydrogenation is given on the use of ruthenium, rhodium and iridium catalysts [29–31]. In view of the significant contribution of rhodium complexes towards catalysis, herein we have also explored the catalytic efficiency of the synthesized Rh(III) complex, $[\text{Rh}(\text{PPh}_3)(\text{L})\text{Cl}_2]$ (**1**) towards transfer hydrogenation of ketones in ^tPrOH.

* Corresponding author.

E-mail address: tapank.mondal@jadavpuruniversity.in (T. Kumar Mondal).

2. Experimental

2.1. Materials

2-(Benzylthio)-N-(pyridin-2-ylmethylene)aniline (L-CH₂Ph) was synthesized following the published procedure [32]. Pyridine-2-carboxaldehyde, 2-aminothiophenol and RhCl₃·3H₂O were purchased from Sigma Aldrich, and used as received. All other chemicals and solvents were of reagent grade and were used without further purification.

2.2. Physical measurements

Microanalyses (C, H, N) were performed using a Perkin-Elmer CHN-2400 elemental analyzer. Electronic spectra were measured on Lambda 750 PerkinElmer spectrophotometer in dichloromethane solution. IR spectra were recorded on RX-1 Perkin Elmer spectrophotometer in the spectral range 4000–400 cm⁻¹ with the samples in the form of KBr pellets. Luminescence property was measured using Shimadzu RF-6000 fluorescence spectrophotometer at room temperature (298 K) in acetonitrile solution by 1 cm path length quartz cell. Fluorescence lifetimes were measured using a time-resolved spectrofluorometer from IBH, UK. The instrument uses a picoseconds diode laser (NanoLed-03, 370 nm) as the excitation source and works on the principle of time-correlated single photon counting [33]. The goodness of fit was evaluated by χ^2 criterion and visual inspection of the residuals of the fitted function to the data. ¹H NMR spectra were recorded in CDCl₃ on Bruker 300 MHz FT-NMR spectrometers in presence of TMS as internal standard. Cyclic voltammograms were recorded using CHI Electrochemical workstation. A platinum wire working electrode, a platinum wire auxiliary electrode and Ag/AgCl reference electrode were used in a standard three-electrode configuration. Tetrabutylammonium hexafluorophosphate (NBu₄PF₆) (0.1 M) was used as the supporting electrolyte and the scan rate used was 50 mV s⁻¹ in CH₂Cl₂ under N₂ atmosphere. ESI mass spectra were recorded on a micro mass Q-TOF mass spectrometer. The one electron oxidized species 1⁺ was generated by exhaustive electrolysis of 1 [34].

The luminescence quantum yield was determined using carbazole as reference with a known ϕ_R of 0.42 in MeCN. The complex and the reference dye were excited at the same wavelength, maintaining nearly equal absorbance (~0.1), and the emission spectra were recorded. The area of the emission spectrum was integrated using the software available in the instrument and the quantum yield is calculated according to the following equation:

$$\phi_S/\phi_R = [A_S / A_R] \times [(Abs)_R / (Abs)_S] \times [\eta_S^2/\eta_R^2]$$

Here, ϕ_S and ϕ_R are the luminescence quantum yield of the sample and reference, respectively. A_S and A_R are the area under the emission spectra of the sample and the reference respectively, $(Abs)_S$ and $(Abs)_R$ are the respective optical densities of the sample and the reference solution at the wavelength of excitation, and η_S and η_R are the values of refractive index for the respective solvent used for the sample and reference.

The yields of catalytic conversion were determined by GC instrument equipped with a flame ionization detector (FID) using a HP-5 column of 30 m length, 0.53 mm diameter and 5.00 μ m film thickness. The column, injector and detector temperatures were 200, 250 and 250 °C respectively. The carrier gas was N₂ (UHP grade) at a flow rate of 30 mL/min. The injection volume of sample was 2 μ L. The oxidation products were identified by GC co-injection with authentic samples.

2.3. Preparation of [Rh(PPh₃)(L)Cl₂] (1)

The reaction mixture containing RhCl₃·3H₂O (0.10 g, 0.38 mmol), L-CH₂Ph (0.101 g, 0.38 mmol) and PPh₃ (0.262 g, 1 mmol) in 20 mL acetonitrile was refluxed for 8 h to yield a deep green solution. The solvent was then removed under reduced pressure. The dried crude product was purified by using silica gel (mesh 60–120) column chromatography. The green band of the complex was eluted by 30% (v/v)

Table 1

Crystallographic data for [Rh(PPh₃)(L)Cl₂] (1).

Formula	C ₃₀ H ₂₄ Cl ₂ N ₂ PRhS
Formula Weight	649.35
Crystal System	Monoclinic
Space group	C2/c
a / Å	33.096(3)
b / Å	11.0554(8)
c / Å	17.9101(14)
β (°)	114.662(4)
V / Å ³	5955.4(8)
Z	8
ρ_{calcd} / g cm ⁻³	1.448
μ / mm ⁻¹	0.898
T / K	293(2)
Radiation / Å	0.71073
hkl range	-42 to 42; -14 to 14; -23 to 23
F(000)	2624
θ range (°)	1.963–27.546
Reflection collected	49,862
Unique reflns (R _{int})	6864
Observed data (I > 2 σ (I))	6044
Data/restraints/parameters	6864 / 0 / 334
R1 ^a , wR2 ^b [I > 2 σ (I)]	0.0238, 0.0593
GOF ^c	1.034
Largest diff. Peak/hole, / e Å ⁻³	0.543 and -0.489

^a $R_1 = \sum (|F_o| - |F_c|) / \sum |F_o|$.

^b $wR_2 = \{ \sum [w(F_o^2 - F_c^2)^2] / \sum [w(F_o^2)^2] \}^{1/2}$, $w = 1/[\sigma^2(F_o^2) + (0.0303P)^2 + 5.6657P]$, where $P = (F_o^2 + 2F_c^2)/3$.

^c $GOF = \{ \sum [w(F_o^2 - F_c^2)^2] / (n-p) \}^{1/2}$, where n = number of measured data and p = number of parameters.

ethyl acetate-petroleum ether mixture. After removal of the solvent under reduced pressure, the solid pure green product was further dried under vacuum. Yield, 0.155 g (63%).

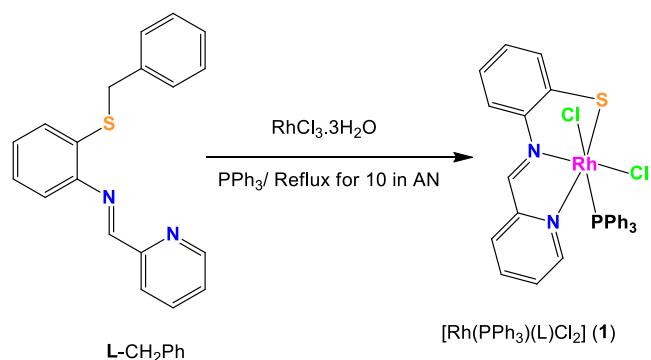
Anal. Calc. for C₃₀H₂₄N₂Cl₂PRhS: Calculated C, 55.49; H, 3.37; N, 4.31 Found: C, 55.35; H, 3.65; N, 4.55. IR (KBr, ν_{max} /cm⁻¹): 1584 (C=N), 747 (S-C). ¹H NMR (CDCl₃, ppm): 8.78 (1H, s, CH = N), 8.66 (1H, d, J = 4.4 Hz), 8.43 (1H, d, J = 8.2 Hz), 7.83 (1H, m), 7.12–7.52 (20H, m). ESI-MS (m/z) calculated for C₃₀H₂₄N₂ClPRhS [M-Cl]⁺ 613.0141, found 613.0157. ¹³C{¹H} NMR (CDCl₃, ppm): 171.2 (C=N), 152.1 (Ar-C), 148.3 (Ar-C), 146.4 (Ar-C), 138.3 (PPh₃-C), 132.4 (PPh₃-CH), 129.4 (PPh₃-CH), 126.3 (Ar-C), 123.8 (Ar-C). ³¹P{¹H} NMR (CDCl₃, ppm): 29.7 (d, ¹J_{Rh-P} = 116.8 Hz, PPh₃). UV-Vis (in CH₂Cl₂), λ_{max} (ϵ , M⁻¹cm⁻¹): 650 (1230), 333 (8751), 267 (25328). E_{1/2}: 0.68 V (ΔE = 88 mV) (E_{pa}: 0.724 V E_{pc}: 0.636 V); E_{pc}: -1.09 V.

2.4. Procedure for catalytic transfer hydrogenation

In a typical experiment the ketone (2 mmol), KOH (0.02 mmol), and complex 1 (0.005 mmol) were added to degassed ⁱPrOH (5 mL), and the mixture was stirred at 80 °C in an inert atmosphere for 6 h. The reaction was then monitored at various time intervals by the use of GC. After the reaction was complete, ⁱPrOH was removed on a rotary evaporator, and the resulting semisolid was extracted with diethyl ether (5 × 5 mL). The combined liquid phase was analyzed by GC using undecane as an internal standard.

2.5. Computational Details

Full geometry optimization of complex 1 was carried out by DFT/B3LYP method [35,36]. All elements except rhodium were assigned the 6-31G(d) basis set. For Rh, LanL2DZ basis set with effective core potential was employed [37–39]. The vibrational frequency calculation was performed to ensure that the optimized geometry represents the local minima and there are only positive eigenvalues. All calculations were performed with Gaussian09 program package [40] with the aid of the GaussView visualization program. Vertical electronic excitations based on B3LYP optimized geometry were computed using the time-



Scheme 1. Synthesis of complex **1** with L-CH₂Ph ligand (where, L-CH₂Ph = 2-(benzylthio)-N-(pyridin-2-ylmethylene)aniline).

dependent density functional theory (TDDFT) formalism [41–43] in CH₂Cl₂ using conductor-like polarizable continuum model (CPCM) [44–46]. The fractional contributions of various groups to each molecular orbital was calculated using GaussSum program [47].

2.6. Crystal structure determination and refinement

Details of crystal analysis, data collection and structure refinement data for [Rh(PPh₃)(L)Cl₂] (**1**) is given in Table 1. Single crystal data collections were performed with an automated Bruker SMART APEX CCD diffractometer using graphite monochromatized Mo-K α radiation ($\lambda = 0.71073 \text{ \AA}$) at 293 °C. Reflection data were recorded using the ω scan technique. The data were integrated using the SAINT [48] program, and the absorption corrections were made with SADABS [48]. The structure was solved by direct method and refined by full-matrix least-squares techniques on F^2 using the SHELXL-2016/6 program [49]. All data were corrected for Lorentz and polarization effects, and the non-hydrogen atoms were refined anisotropically. Hydrogen atoms were included in the refinement process as per the riding model. The electron density map also showed the presence of some unassignable peaks, which were removed by SQUEEZE method [50].

3. Results and discussion

3.1. Synthesis and spectral characterization

The Rh(III)-phosphine complex, [Rh(PPh₃)(L)Cl₂] (**1**) was synthesized by the reaction of RhCl₃, 2-(benzylthio)-N-(pyridine-2-ylmethylene)aniline (L-CH₂Ph) and excess PPh₃ in acetonitrile under refluxing condition (scheme 1). The colour of the reaction mixture was changed from red to green. In the course of the reaction benzylic C–S bond of thioether containing L-CH₂Ph ligand is cleaved and L binds to the rhodium(III) centre using pyridyl-N, imine-N and thiophenolato-S atoms. The complex was thoroughly characterized by several spectroscopic techniques. In IR spectra, the free ligand (L-CH₂Ph) stretching at 1621 cm⁻¹ and 776 cm⁻¹ corresponding to imine $\nu(\text{C}=\text{N})$ and $\nu(\text{C}-\text{S})$ are shifted to 1584 cm⁻¹ and 747 cm⁻¹ in the complex supporting the coordination of the ligand to the metal. The ¹H NMR peak at 4.16 ppm corresponding to benzylic protons (–CH₂) is absent in metal complex indicating the C–S bond cleavage (experimental section). The singlet peak corresponding to imine proton (HC = N) appears at 8.78 ppm. Aromatic protons appeared as multiplet due to the presence of PPh₃ group. The overlapping of many proton resonances due to their similar chemical shifts has prevented identification of individual proton signals of the aromatic protons; though the spectra shows the calculated number of equivalent aromatic protons.

The solution spectrum of the rhodium(III) complex, [Rh(PPh₃)(L)Cl₂] (**1**) in dichloromethane exhibits low energy peak at 650 nm (ϵ , 1230 M⁻¹cm⁻¹) along with two moderately intense bands at 333 (ϵ ,

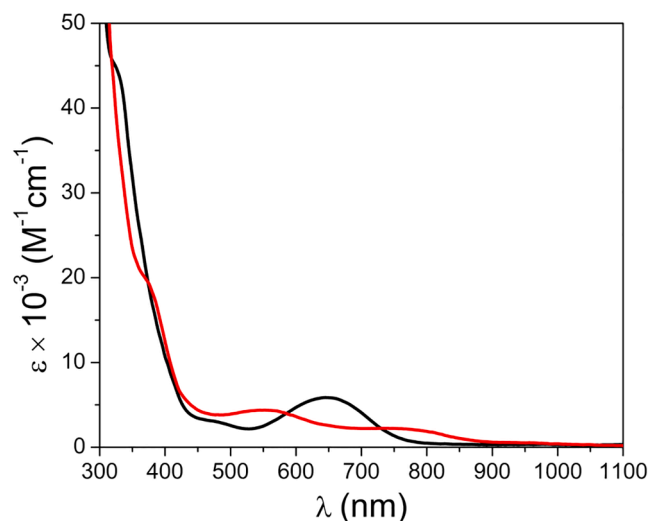


Fig. 1. UV-vis-NIR spectra of complex **1** and electrogenerated complex **1**⁺ in CH₂Cl₂.

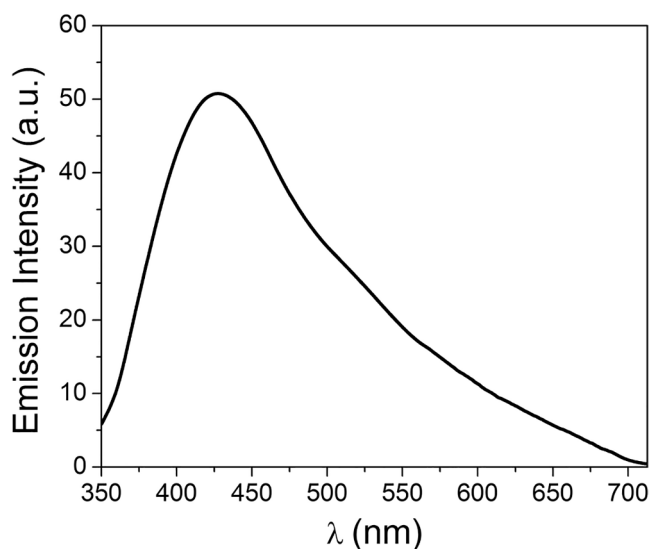


Fig. 2. Luminescence spectrum of **1** in CH₂Cl₂ ($\lambda_{\text{ex}} = 333 \text{ nm}$).

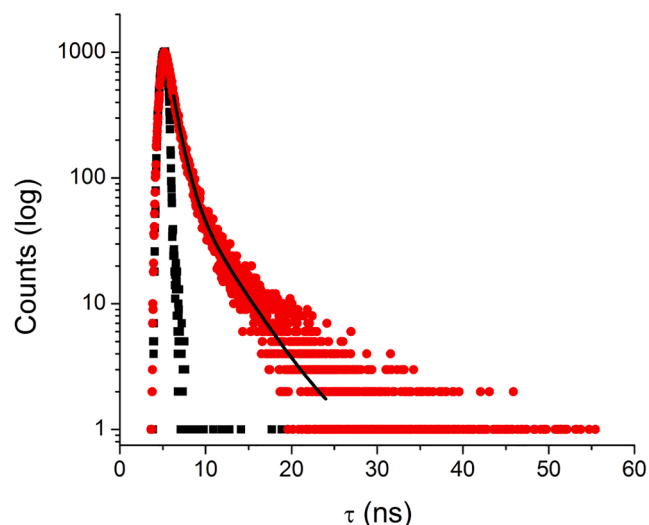


Fig. 3. Exponential decay profile of **1** in CH₂Cl₂ ($\tau = 1.57 \text{ ns}$).

Table 2
X-ray and calculated bond distances (Å) and angles (°) of **1** and **1⁺**.

Bond (Å)	X-ray		Calc.	
	1		1	1⁺
Rh1-Cl1	2.3521(5)		2.412	2.383
Rh1-Cl2	2.4353(5)		2.433	2.473
Rh1-S1	2.3054(5)		2.367	2.317
Rh1-P1	2.2902(5)		2.413	2.416
Rh1-N1	2.1076(15)		2.141	2.102
Rh1-N2	2.0001(14)		2.041	2.047
Angles (°)				
N1- Rh1- N2	79.99(6)		79.964	79.963
N1-Rh1- P1	94.57(4)		96.059	95.723
N1- Rh1- S1	166.12(4)		165.034	161.301
N1- Rh1-Cl1	97.00(4)		95.391	96.493
N1- Rh1-Cl2	86.53(4)		85.227	88.806
N2-Rh1- P1	94.15(4)		95.986	95.852
N2- Rh1- S1	86.28(4)		85.523	85.442
N2- Rh1-Cl1	173.25(4)		173.150	173.303
N2- Rh1-Cl2	84.97(4)		84.507	84.612
P1-Rh1- S1	88.413(19)		88.992	97.345
P1-Rh1-Cl1	92.109(18)		89.483	90.135
P1-Rh1-Cl2	178.458(18)		178.648	175.459
S1-Rh1-Cl1	96.434(18)		98.728	96.790
S1-Rh1-Cl2	90.27(2)		89.793	78.178
Cl1- Rh1-Cl2	88.831(19)		90.116	89.649

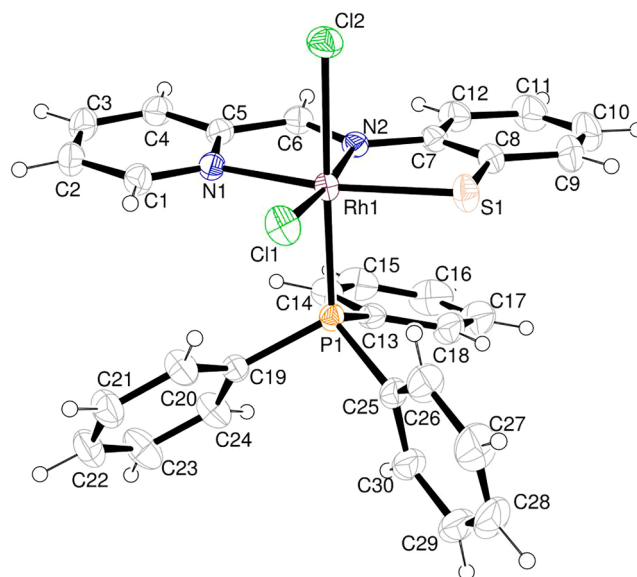


Fig. 4. ORTEP plots of **1** with 35% ellipsoidal probability.

8751 $\text{M}^{-1}\text{cm}^{-1}$) and 267 nm (ϵ , 25328 $\text{M}^{-1}\text{cm}^{-1}$) (Fig. 1). In addition, a low energy band as shoulder is also appeared at 479 nm. Upon excitation at 333 nm, an emission band at 432 nm with emission quantum yield (ϕ) = 0.015 is observed in CH_2Cl_2 (Fig. 2). Lifetime data of the complex was taken at 298 K in CH_2Cl_2 solution when excited at 370 nm. The fluorescence decay curve was deconvoluted with respect to the lamp profile. The observed fluorescence decay fits with bi-exponential nature (Fig. 3). We have used mean fluorescence lifetime ($\tau_f = a_1\tau_1 + a_2\tau_2$, where a_1 and a_2 are relative amplitude of decay process) to study the excited state stability of the complex. The fluorescence lifetime of the complex is found to be 1.57 ns.

3.2. Molecular structure

Single crystals of **1** were grown by layering *n*-hexane and dichloromethane solution of the complex. Selected bond distances and bond angles of the complex are summarized in Table 2. The molecular structure with atomic numbering is represented in Fig. 4. After cleavage of benzyl fragment, the uninegative ligand binds in a tridentate fashion through pyridyl-N, imine-N and thiophenolato-S atoms to the rhodium (III) center. The geometry about rhodium(III) is significantly deviated from ideal octahedron. The deviation of coordination sphere from ideal octahedron is reflected from small bite angles of the five membered chelate rings, Rh1-N1-C5-C6-N2, 79.99(6)° and Rh1-N2-C7-C8-S1, 86.28(4)°. The Rh-N(pyridyl) bond, Rh1-N1, 2.1076(15) Å is much more elongated than the Rh-N(imine) bond distance, Rh1-N2, 2.0001(14) Å, while the reverse Re-N bond distances was reported previously [51]. The Rh1-S1 bond distance, 2.3054(5) Å is comparable to the reported Rh-S bond distances [52–54]. Rh1-Cl1 and Rh1-Cl2 bond lengths are found to be 2.3521(5) and 2.4353(5) Å respectively. A 2D supra-molecular structure is formed by inter-molecular $\pi\cdots\pi$ interactions between phenyl ring (Cg(4): C7-C8-C9-C10-C11-C12) and pyridyl ring (Cg(3): N1-C1-C2-C3-C4-C5) of the adjacent molecule with Cg-Cg distance of 3.7462(14) Å. In addition, strong intra-molecular $\pi\cdots\pi$ interactions are found between phenyl ring of the ligand (Cg(4)) and one of the phenyl ring of PPh_3 (Cg(5): C13-C14-C15-C16-C17-C18) with Cg-Cg distance of 3.7527(14) Å (Fig. 5).

3.3. DFT calculation and electronic structure

The geometry of the **1** and the oxidized form, **1⁺** were optimized to interpret the electronic structures in native as well as in the oxidized state

by DFT/B3LYP method. The optimized bond distances and angles are well correlated with the X-ray crystal structure data in the native state. Upon oxidation, significant change in Rh1-S1 bond distance is observed (Table 2).

The energy and compositions of selected molecular orbitals of **1** are summarized in Table 3. Contour plots of selected molecular orbitals are shown in Fig. 6. The higher energy occupied molecular orbital (HOMO) has 90% contribution of L (S, 53%) along with reduced contribution (06%) of $d\pi(\text{Rh})$. The HOMO-1 to HOMO-4 have major contribution of $p\pi(\text{Cl})$ orbitals (61–89%) along with significant contribution of $d\pi(\text{Rh})$ orbitals. The low lying virtual orbital, LUMO has 95% $\pi^*(\text{L})$ character while LUMO + 1 and LUMO + 2 have significant contribution of $d\pi(\text{Rh})$ orbitals. The HOMO to LUMO energy gap in the complex is found to be 2.23 eV.

To understand the electronic structure in the oxidized state (**1⁺**), we have considered the effect in changes in the energies and compositions of molecular orbitals of the complex in the oxidized form. Energy and composition of selected molecular orbitals are summarized in Table S1 and Table S2 for α and β spin respectively. The contour plots of selected molecular orbitals are shown in Fig. S1 and Fig. S2 for α and β spin respectively. The Spin density of the oxidized species is well distributed on the ligand with major contribution of S atom (63%) (Fig. 7).

3.4. TDDFT calculation and electronic spectra

The solution spectrum of **1** in dichloromethane exhibits peaks at 650 nm (ϵ , 1230 $\text{M}^{-1}\text{cm}^{-1}$) along with a shoulder at 479 nm. In addition, two moderately intense bands at 333 (ϵ , 8751 $\text{M}^{-1}\text{cm}^{-1}$) and 267 nm (ϵ , 25328 $\text{M}^{-1}\text{cm}^{-1}$) are observed (Fig. 1). To interpret the electronic transitions in the complex, TDDFT calculation was carried out by TDDFT/CPCM method in dichloromethane. The band at 650 nm corresponds to the HOMO \rightarrow LUMO transition ($\lambda = 666$ nm; $f = 0.034$) having ILCT character (Table 4). The peak appeared as shoulder at 479 nm has mixed XLCT (halogen to ligand charge transfer transition) and MLCT (metal to ligand charge transfer transitions) character. The high energy band at 333 nm corresponds to the $\pi(\text{L}) \rightarrow \pi^*(\text{L})$ transition (ILCT) in the complex.

3.5. Electrochemistry

The electrochemical behavior of the complex was investigated by cyclic voltammetry (CV) in dichloromethane solvent using tetra-*n*-

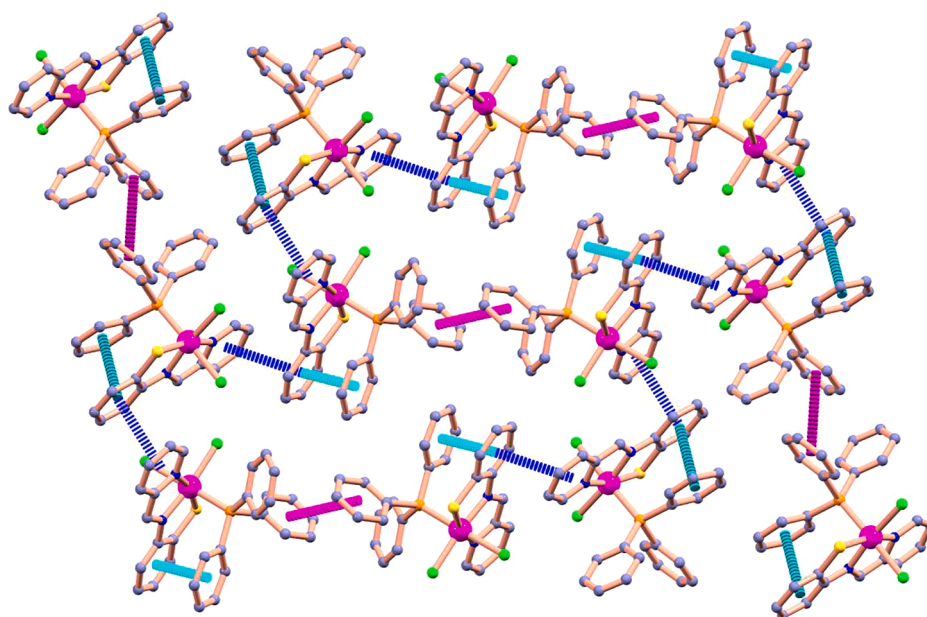


Fig. 5. 2D-supramolecular structure of **1** by intra- and inter-molecular $\pi \dots \pi$ interactions.

Table 3

Energy and composition of selected molecular orbitals of **1**.

MO	Energy (eV)	% of composition				
		L	Σ Cl	Rh	PPh3	
LUMO + 5	-0.77	05	02	04	89	
LUMO + 4	-0.89	04	0	0	96	
LUMO + 3	-1.37	86	02	07	05	
LUMO + 2	-1.52	46	09	44	01	
LUMO + 1	-1.77	09	20	37	33	
LUMO	-2.80	95	01	03	01	
HOMO	-5.03	90(S, 53)	02	06	02	
HOMO-1	-5.81	04	84	11	01	
HOMO-2	-5.83	01	89	08	02	
HOMO-3	-5.98	03	70	17	10	
HOMO-4	-6.10	12	61	25	02	
HOMO-5	-6.63	74	07	07	12	
HOMO-6	-6.71	20	17	06	57	
HOMO-7	-6.79	04	02	01	93	
HOMO-8	-6.92	11	09	05	75	
HOMO-9	-7.11	06	02	02	90	
HOMO-10	-7.20	45	20	14	21	

butylammonium hexafluorophosphate (NBu₄PF₆) (0.1 M) as supporting electrolyte and a Ag/AgCl reference electrode. The complex exhibits a reversible oxidation couple with E_{1/2}, 0.68 V ($\Delta E = 88$ mV) along with an irreversible reduction peak at -1.09 V in the potential range of -1.5 to 1.0 V versus Ag/AgCl electrode (Fig. 8). The oxidation couple may be assigned to Rh(III)/Rh(IV) oxidation in the complex [55,56]. But the composition of HOMO of the complex has 90% ligand character with major contribution of $p\pi(S)$ orbitals (53%). So, we may consider the ligand centered oxidation on thiophenolato-S to form thiyl radical in the complex [14,15,17]. The irreversible cathodic peak at -1.09 V may corresponds to the reduction of coordinated ligand (L) as the composition of LUMO has 95% $\pi^*(L)$ character in the complex.

Moreover, for better understand the oxidation process in the complex, we have calculated the Mulliken atomic charges by DFT/B3LYP method of **1** and **1**⁺ (Table 5). Mulliken atomic charges of **1** and **1**⁺ species clearly show that there is significant enhancement of positive charge on S atom compared to rhodium atom in **1**⁺. Again, the possibility of formation of thiyl radical is further supported by the 63% spin density on S atom in comparison to 3% on rhodium in **1**⁺ (Fig. 7). So, the

oxidation is assigned as thiophenolato to thiyl radical formation over the minor possibility of Rh(III)/Rh(IV) process in the complex. The electronically generated oxidized species by extensive bulk electrolysis at constant potential at 0.7 V exhibits sharp changes in the UV-VIS-NIR spectra. The low energy band at 655 nm in the native state is red shifted and observed at 766 nm. In addition, a new band at 564 nm is developed during oxidation (Fig. 1).

3.6. Catalytic transfer hydrogenation reactions

Rhodium complex mediated transfer hydrogenation reactions are discovered to be very effective catalytic systems in which hydrogen is transferred from one organic molecule to another molecule. The present Rh(III) complex **1** was taken as catalyst and the catalytic activity in transfer hydrogenation of different aromatic and aliphatic ketones in presence of ⁱPrOH and KOH as promoter was carried out.

The transfer hydrogenation of acetophenone was standardized with the variation of base, catalyst loading, reaction time, temperature and results are summarized in Table 6. When the amount of catalyst

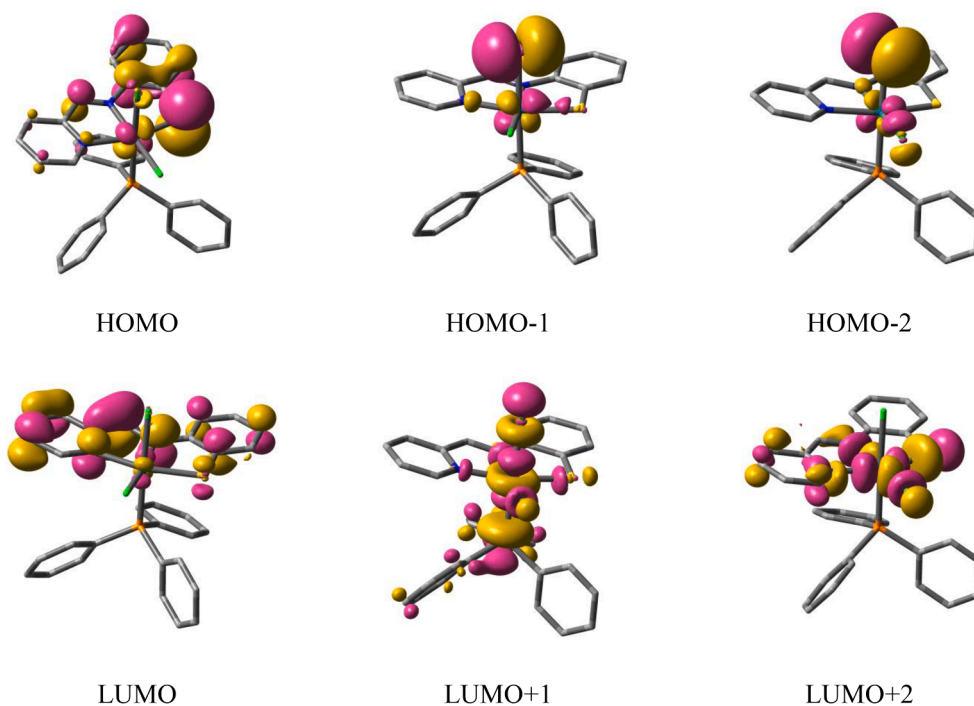


Fig. 6. Contour plots of some selected molecular orbitals of **1**. Isodensity value 0.04 e Bohr^{-3} .

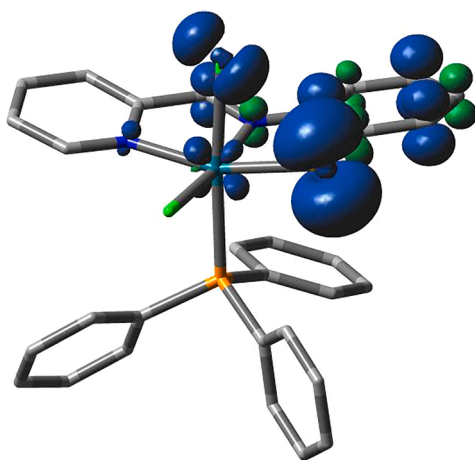


Fig. 7. Spin density plot of 1^+ (Rh, 3%; S, 63%). Isodensity value $0.004 \text{ e Bohr}^{-3}$.

Table 4

Vertical electronic excitations calculated by TDDFT/CPCM method of **1** in CH_2Cl_2 .

Excitation (eV)	$\lambda_{\text{excitation}}$ (nm)	Osc. Strength (f)	Key transitions	Character	$\lambda_{\text{expt.}}$ (nm)
1.8612	666.2	0.0343	(98%) HOMO → LUMO	$p\pi(\text{S}) \rightarrow \pi^*(\text{L})$ ILCT	655
2.6106	474.92	0.0113	(86%) HOMO-3 → LUMO	$p\pi(\text{Cl})/d\pi(\text{Rh}) \rightarrow \pi^*(\text{L})$ XLCT/MLCT	479
3.4942	354.83	0.0781	(75%) HOMO-5 → LUMO	$\pi(\text{L}) \rightarrow \pi^*(\text{L})$, ILCT	333

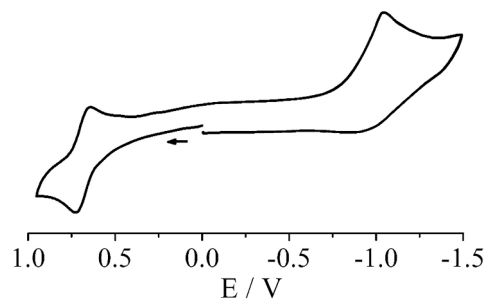


Fig. 8. Cyclic voltammogram of **1** in CH_2Cl_2 with respect to Ag/AgCl reference electrode ([NBu₄PF₆] was used as the supporting electrolyte).

Table 5

Mulliken atomic charges calculated by DFT/B3LYP method of **1** and 1^+ .

Atoms	1	1^+
Rh1	-0.301	-0.352
Cl1	-0.275	-0.190
Cl2	-0.245	-0.148
P1	0.694	0.707
S1	0.109	0.366
N1	-0.471	-0.495
N2	-0.501	-0.514

increased from 0.10 to 0.15, 0.20 and 0.25 mol%, the yields of 1-phenylethyl alcohol were increased from 72 to 85, 94 and 98% respectively. Further, the reaction was carried out in absence of catalyst **1** and with RhCl_3 . In both the cases no significant catalytic conversions were observed. With the increase of reaction time from 1 to 6 h, the yield was increased from 51 to 98%. Reaction time was also played a vital role, with the increase of temperature from 40 to 80 °C the yields of 1-phenylethyl alcohol increased from 25 to 98%. The bases play a significant role in transfer hydrogenation reaction and without any base the reaction was hardly proceeded. In the catalytic cycle, probably the Rh-Cl bond is

Table 6
Optimization of transfer hydrogenation of acetophenone^a by complex 1.

Entry	Amount of cat. (mol%)	Base used	Amount of base (mol%)	Temp. (°C)	Time (h)	Yield (%) ^b
1	0.10	KOH	1.0	80	6	72
2	0.15	KOH	1.0	80	6	85
3	0.20	KOH	1.0	80	6	94
4	0.25	KOH	1.0	80	6	98
5	0.25	Na ₂ CO ₃	1.0	80	6	73
6	0.25	NaOAc	1.0	80	6	45
7	0.25	KO ^t Bu	1.0	80	6	82
8	0.25	KOH	0.5	80	6	79
9	0.25	KOH	0.8	80	6	92
10	0.25	KOH	1.0	40	6	25
11	0.25	KOH	1.0	60	6	54
12	0.25	KOH	1.0	80	1	51
13	0.25	KOH	1.0	80	2	72
14	0.25	KOH	1.0	80	3	81
15	0.25	KOH	1.0	80	4	88
16	0.25	KOH	1.0	80	5	95

^a Reaction condition: acetophenone (2 mmol), ⁱPrOH 5 mL.

^b Conversions were determined by GC with undecane as an internal standard and were reported mean values of three runs.

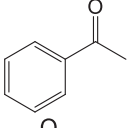
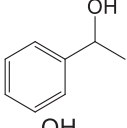
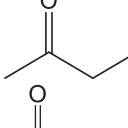
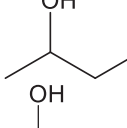
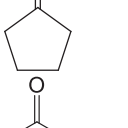
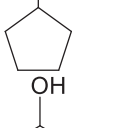
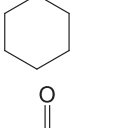
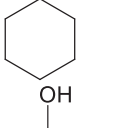
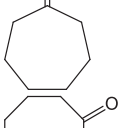
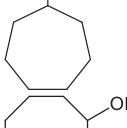
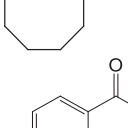
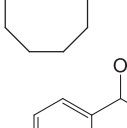
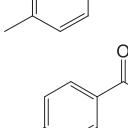
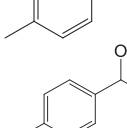
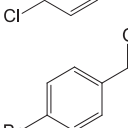
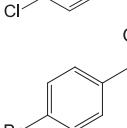
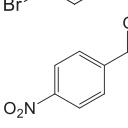
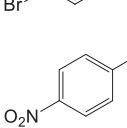
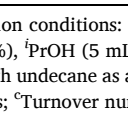
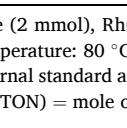
cleaved and formation of new intermediate complex having Rh-H bond is taking place which is then effectively reduced the ketones to their corresponding alcohols [31]. In general, the catalytic conversion of transfer hydrogenation reactions is strongly dependent on the base strength – the stronger the bases higher the yields [57–59]. In present case, reaction was proceeded very well with strong base (KOH), while for weak bases like Na₂CO₃ and NaOAc, the yields were very poor.

In recent years we have successfully synthesized several rhodium (III)-triphenylphosphine complexes and explored their catalytic efficiency towards transfer hydrogenation of ketones, a moderate to high catalytic conversions (85–98%) were observed under optimum reaction conditions [19–21]. Kühn et al. observed 86–100% yields for heterocyclic carbene rhodium(I) complexes [60]. Karakaş and co-workers used ionic liquid based R(I) complexes as efficient catalysts and observed 90–99% yields [61]. The results of transfer hydrogenation by the present Rh(III) complex 1 under are summarized in Table 7. For aliphatic ketones like 2-butanone, cyclopentanone, cyclohexanone, cycloheptanone and cyclooctanone the conversions to their corresponding alcohols were achieved to 89–96%. While for aromatic ketones with electron donating or withdrawing groups excellent yields were observed (96–98%).

4. Conclusion

Herein, we have synthesized new rhodium(III) complex, [Rh(L)(PPh₃)Cl₂] (1) by C–S bond cleavage of thioether containing ligand, L-CH₂Ph. The complex is thoroughly characterized by several spectroscopic techniques and the distorted octahedral geometry is confirmed by single crystal X-ray study. The complex exhibits ligand based thiophenolato to thiyl radical oxidation over the alternate possibility of Rh(III)/Rh(IV) process. The complex effectively catalyzed the transfer hydrogenation reaction of ketones with moderate to high yields (89–98%) in ⁱPrOH. Electronic structure, solution spectrum and redox properties are well interpreted by DFT and TDDFT calculations.

Table 7
Transfer hydrogenation of various ketones using complex 1.^a

Entry	Ketones	Alcohols	Conversion (%) ^b	TON ^c
1			98	392
2			92	368
3			94	376
4			96	384
5			93	372
6			89	356
7			97	388
8			98	392
9			96	384
10			98	392

^a Reaction conditions: ketone (2 mmol), Rh(III) complex (0.25 mol%), KOH (1.0 mol%), ⁱPrOH (5 mL), temperature: 80 °C; ^bConversions were determined by GC with undecane as an internal standard and were reported mean values of three runs; ^cTurnover number (TON) = mole of product/mol of catalyst.

CRediT authorship contribution statement

Sujan Biswas: Investigation, Writing - original draft. **Chandan Kumar Manna:** Investigation. **Rahul Naskar:** Investigation. **Akash Das:** Investigation. **Tapan Kumar Mondal:** Supervision, Writing - review & editing.

Declaration of Competing Interest

The authors declare that they have no known competing financial interests or personal relationships that could have appeared to influence the work reported in this paper.

Acknowledgment

Financial support received from the Science and Engineering Research Board (SERB) (No. EEQ/2018/000266), New Delhi, India is gratefully acknowledged. TKM is also grateful to RUSA II programme for financial support. S. Biswas and R. Naskar are thankful to UGC, New Delhi, India for fellowship.

Appendix A. Supplementary data

Supplementary data to this article can be found online at <https://doi.org/10.1016/j.ica.2020.120096>.

References

- [1] T.-Y. Luh, C.-F. Lee, Dithioacetals as zwitterion synthons, *Eur. J. Org. Chem.* 3875–3885 (2005).
- [2] I.P. Beletskaya, V.P. Ananikov, Transition-metal-catalyzed C–S, C–Se, and C–Te bond formation via cross-coupling and atom-economic addition reactions, *Chem. Rev.* 111 (2011) 1596–1636.
- [3] L. Wang, W. He, Z. Yu, Transition-metal mediated carbon–sulfur bond activation and transformations, *Chem. Soc. Rev.* 42 (2013) 599–621.
- [4] R. Tan, D. Song, C–H and C–S activations of quinoline-functionalized thiophenes by platinum complexes, *Organometallics* 30 (2011) 1637–1645.
- [5] S. Kundu, W.W. Brennessel, W.D. Jones, C–S bond activation of thioesters using platinum(0), *Organometallics* 30 (2011) 5147–5154.
- [6] M.R. Grochowski, T. Li, W.W. Brennessel, W.D. Jones, Competitive carbon–sulfur vs carbon–carbon bond activation of 2-cyanothiophene with [Ni(dippe)H]₂, *J. Am. Chem. Soc.* 132 (2010) 12412–12421.
- [7] Y. Miyazaki, K. Oohora, T. Hayashi, Methane generation via intraprotein C–S bond cleavage in cytochrome b562 reconstituted with nickel didehydrocorrin, *J. Organomet. Chem.* 901 (2019) 120945.
- [8] J. Lou, Q. Wang, P. Wu, H. Wang, Y.-G. Zhou, Z. Yu, Transition-metal mediated carbon–sulfur bond activation and transformations: an update, *Chem. Soc. Rev.* 49 (2020) 4307–4359.
- [9] K. Ray, S.D. George, E.I. Solomon, K. Wiegardt, F. Neese, Description of the ground-state covalencies of the bis(dithiolato) transition-metal complexes from X-ray absorption spectroscopy and time-dependent density-functional calculations, *Chem. Eur. J.* 13 (2007) 2783–2797.
- [10] M. Tamura, K. Tsuge, A. Igashira-Kamiyama, T. Konno, Bis(bipyridine)ruthenium (II) complexes with an aliphatic sulfinato donor: synthesis, characterization, and properties, *Inorg. Chem.* 50 (2011) 4764–4771.
- [11] S.G. Modha, V.P. Mehta, E. Van der Eycken, Transition metal-catalyzed C–C bond formation via C–S bond cleavage: an overview, *Chem. Soc. Rev.* 42 (2013) 5042–5055.
- [12] L.R. Hanton, K. Lee, C–S bond cleavage by chloride in a thioether N₂S₂ complex of platinum, *Inorg. Chem.* 38 (1999) 1634–1637.
- [13] S. Mandal, N. Paul, P. Banerjee, T.K. Mondal, S. Goswami, 1,4-Alkyl migration associated with simultaneous S–C bond cleavage and N–C bond formation in platinum complexes of 2-aminothioethers. Characterization of intramolecular interligand charge transfer phenomenon, *Dalton Trans.* 39 (2010) 2717–2726.
- [14] K. Pramanik, U. Das, B. Adhikary, D. Chopra, H. Stoeckli-Evans, RhCl₃-assisted C–H and C–S bond scissions: isomeric self-association of organorhodium(III) thiolato complex. synthesis, structure, and electrochemistry, *Inorg. Chem.* 47 (2008) 429–438.
- [15] U. Das, T. Ghorui, B. Adhikary, S. Roy, S. Pramanik, K. Pramanik, Iridium-mediated C–S bond activation and transformation: organoiridium(III) thioether, thiolato, sulfinato and thyl radical compounds. Synthesis, mechanistic, spectral, electrochemical and theoretical aspects, *Dalton Trans.* 44 (2015) 8625–8639.
- [16] S. Acharya, P. Bandyopadhyay, P. Das, S. Biswas, A.N. Biswas, Alkyl-sulfur versus aryl-sulfur bond cleavage in tridentate alkylthiophenylazonaphthols by group 9 metal ions, *J. Organomet. Chem.* 866 (2018) 13–20.
- [17] S. Biswas, P. Roy, T.K. Mondal, Synthesis of palladium(II) complex with NNS donor Schiff base ligand via C–S bond cleavage: X-ray structure, electrochemistry and DFT computation, *J. Mol. Struct.* 1142 (2017) 110–115.
- [18] P. Roy, D. Sarkar, P. Ghosh, C.K. Manna, N. Murmu, T.K. Mondal, Synthesis of luminescent rhodium(III) cyclometalated complex by sp²(C)–S bond activation: application as catalyst in transfer hydrogenation of ketones and live cell imaging, *J. Mol. Struct.* 1204 (2020) 127524.
- [19] P. Roy, R. Naskar, C.K. Manna, T.K. Mondal, Synthesis of thiolato bridged dimeric rhodium(III) triphenylphosphine complex via C–S bond cleavage: X-ray structure, DFT computation and catalytic evaluation towards transfer hydrogenation of ketones, *J. Mol. Struct.* 1198 (2019) 126932.
- [20] P. Roy, C.K. Manna, R. Naskar, T.K. Mondal, Synthesis of a rhodium(III) triphenylphosphine complex via C–S bond cleavage of an azo-thioether ligand: X-ray structure, electrochemistry and catalysis towards transfer hydrogenation of ketones, *Polyhedron* 158 (2019) 208–214.
- [21] S. Biswas, D. Sarkar, S. Kundu, P. Roy, T.K. Mondal, Rhodium(III)-triphenylphosphine complex with NNS donor thioether containing Schiff base ligand: synthesis, spectra, electrochemistry and catalytic activity, *J. Mol. Struct.* 1099 (2015) 297–303.
- [22] D. Wang, D. Astruc, The golden age of transfer hydrogenation, *Chem. Rev.* 115 (2015) 6621–6686.
- [23] M. Yoshimura, S. Tanaka, M. Kitamura, Recent topics in catalytic asymmetric hydrogenation of ketones, *Tetrahedron Lett.* 55 (2014) 3635–3640.
- [24] J. Ito, H. Nishiyama, Recent topics of transfer hydrogenation, *Tetrahedron Lett.* 55 (2014) 3133–3146.
- [25] R. Malacea, R. Poli, E. Manoury, Asymmetric hydrosilylation, transfer hydrogenation and hydrogenation of ketones catalyzed by iridium complexes, *Coord. Chem. Rev.* 254 (2010) 729–752.
- [26] T. Ikariya, A.J. Blacker, Asymmetric transfer hydrogenation of ketones with bifunctional transition metal-based molecular catalysts, *Acc. Chem. Res.* 40 (2007) 1300–1308.
- [27] J.S.M. Samec, J.E. Bäckvall, P.G. Andersson, P. Brandt, Mechanistic aspects of transition metal-catalyzed hydrogen transfer reactions, *Chem. Soc. Rev.* 35 (2006) 237–248.
- [28] J. Magano, J.R. Dunetz, Large-scale carbonyl reductions in the pharmaceutical industry, *Org. Process Res. Dev.* 16 (2012) 1156–1184.
- [29] X.-H. Zhu, L.-H. Cai, C.-X. Wang, Y.-N. Wang, X.-Q. Guo, X.-F. Hou, Efficient and versatile transfer hydrogenation catalysts: Iridium (III) and ruthenium (II) complexes with 4-acetylbenzyl-N-heterocyclic carbenes, *J. Mol. Catal. A Chem.* 393 (2014) 134–141.
- [30] B. He, P. Phansavath, V. Ratovelomanana-Vidal, Rhodium-catalyzed asymmetric transfer hydrogenation of 4-quinolone derivatives, *Org. Chem. Front.* 2 (2020) 975–979.
- [31] O. Prakash, P. Singh, G. Mukherjee, A.K. Singh, Efficient catalysis of transfer hydrogenation of ketones and oxidation of alcohols with newly designed half-sandwich rhodium(III) and iridium(III) complexes of half-pincer chalcogenated pyridines, *Organometallics* 31 (2012) 3379–3388.
- [32] P. Pattanayak, D. Patra, P. Brandão, D. Mal, V. Felix, Synthesis and characterization of palladium (II) complex of Schiff base ligand: CS bond cleavage and catalytic activity, *Inorg. Chem. Commun.* 53 (2015) 68–71.
- [33] B. Valuer, *Molecular Fluorescence: Principles and Applications*, Wiley-VCH, Weinheim, 2001.
- [34] N.D. Paul, S. Samanta, T.K. Mondal, S. Goswami, Examples of reductive azo cleavage and oxidative azo bond formation on Re₂(CO)₁₀ template: isolation and characterization of Re(III) complexes of new azo-aromatic ligands, *Inorg. Chem.* 50 (2011) 7886–7893.
- [35] A.D. Becke, Density-functional thermochemistry. III. The role of exact exchange, *J. Chem. Phys.* 98 (1993) 5648–5652.
- [36] C. Lee, W. Yang, R.G. Parr, Development of the Colle-Salvetti correlation-energy formula into a functional of the electron density, *Phys. Rev. B* 37 (1988) 785–789.
- [37] P.J. Hay, W.R. Wadt, Ab initio effective core potentials for molecular calculations. Potentials for the transition metal atoms Sc to Hg, *J. Chem. Phys.* 82 (1985) 270–283.
- [38] W.R. Wadt, P.J. Hay, Ab initio effective core potentials for molecular calculations. Potentials for main group elements Na to Bi, *J. Chem. Phys.* 82 (1985) 284–298.
- [39] P.J. Hay, W.R. Wadt, Ab initio effective core potentials for molecular calculations. Potentials for K to Au including the outermost core orbitals, *J. Chem. Phys.* 82 (1985) 299–310.
- [40] Gaussian 09, Revision D.01, M. J. Frisch, G. W. Trucks, H. B. Schlegel, G. E. Scuseria, M. A. Robb, J. R. Cheeseman, G. Scalmani, V. Barone, B. Mennucci, G. A. Petersson, H. Nakatsuji, M. Caricato, X. Li, H. P. Hratchian, A. F. Izmaylov, J. Bloino, G. Zheng, J. L. Sonnenberg, M. Hada, M. Ehara, K. Toyota, R. Fukuda, J. Hasegawa, M. Ishida, T. Nakajima, Y. Honda, O. Kitao, H. Nakai, T. Vreven, J. A. Montgomery, Jr., J. E. Peralta, F. Ogliaro, M. Bearpark, J. J. Heyd, E. Brothers, K. N. Kudin, V. N. Staroverov, R. Kobayashi, J. Normand, K. Raghavachari, A. Rendell, J. C. Burant, S. S. Iyengar, J. Tomasi, M. Cossi, N. Rega, J. M. Millam, M. Klene, J. E. Knox, J. B. Cross, V. Bakken, C. Adamo, J. Jaramillo, R. Gomperts, R. E. Stratmann, O. Yazyev, A. J. Austin, R. Cammi, C. Pomelli, J. W. Ochterski, R. L. Martin, K. Morokuma, V. G. Zakrzewski, G. A. Voth, P. Salvador, J. J. Dannenberg, S. Dapprich, A. D. Daniels, Ö. Farkas, J. B. Foresman, J. V. Ortiz, J. Cioslowski, and D. J. Fox, Gaussian, Inc., Wallingford CT (2009).
- [41] R. Bauernschmitt, R. Ahlrichs, Treatment of electronic excitations within the adiabatic approximation of time dependent density functional theory, *Chem. Phys. Lett.* 256 (1996) 454–464.
- [42] R.E. Stratmann, G.E. Scuseria, M.J. Frisch, An efficient implementation of time-dependent density-functional theory for the calculation of excitation energies of large molecules, *J. Chem. Phys.* 109 (1998) 8218–8224.
- [43] M.E. Casida, C. Jamorski, K.C. Casida, D.R. Salahub, Molecular excitation energies to high-lying bound states from time-dependent density-functional response theory: characterization and correction of the time-dependent local density approximation ionization threshold, *J. Chem. Phys.* 108 (1998) 4439–4449.
- [44] V. Barone, M. Cossi, Quantum calculation of molecular energies and energy gradients in solution by a conductor solvent model, *J. Phys. Chem. A* 102 (1998) 1995–2001.
- [45] M. Cossi, V. Barone, Time-dependent density functional theory for molecules in liquid solutions, *J. Chem. Phys.* 115 (2001) 4708–4717.

- [46] M. Cossi, N. Rega, G. Scalmani, V. Barone, Energies, structures, and electronic properties of molecules in solution with the C-PCM solvation model, *J. Comput. Chem.* 24 (2003) 669–681.
- [47] N.M. O'Boyle, A.L. Tenderholt, K.M. Langner, cclib: a library for package-independent computational chemistry algorithms, *J. Comput. Chem.* 29 (2008) 839–845.
- [48] SAINT (version 6.02), SADABS (version 2.03); Bruker AXS Inc., Madison, WI (2002).
- [49] G.M. Sheldrick, A short history of SHELX, *Acta Crystallogr. A* 64 (2008) 112–122.
- [50] A.L. Spek, Single-crystal structure validation with the program PLATON, *J. Appl. Crystallogr.* 36 (2003) 7–13.
- [51] M.S. Jana, A.K. Pramanik, S. Kundu, D. Sarkar, T.K. Mondal, fac-Tricarbonyl rhenium(I) complexes of 2-(alkylthio)-N-((pyridine-2-yl)methylene)benzenamine: synthesis, spectroscopic characterization, X-ray structure and DFT calculation, *Inorg. Chim. Acta* 399 (2013) 138–145.
- [52] M. Hirotsu, A. Kobayashi, T. Yoshimura, T. Konno, Rhodium(III) complexes with thiolate and thioether ligands derived from fac(S)-[Rh(aet)₃] (aet = 2-aminoethanethiolate): selective formation, characterization and properties, *J. Chem. Soc., Dalton Trans.* (2002) 878–884.
- [53] A. Labande, J.-C. Daran, N.J. Long, A.J.P. White, R. Poli, Rhodium(III) and ruthenium(II) complexes of redox-active, chelating N-heterocyclic carbene/thioether ligands, *New J. Chem.* 35 (2011) 2162–2168.
- [54] D. Sardar, P. Datta, P. Mitra, C. Sinha, Rhodium(III) and iridium(III) complexes of thioaryazoimidazoles: synthesis, structure, spectral characterization, electrochemistry and DFT calculation, *Polyhedron* 29 (2010) 3170–3177.
- [55] S.K. Seth, S. Mandal, P. Purkayastha, P. Gupta, Cyclometalated mono and dinuclear rhodium(III) and iridium(III) complexes with imidazolyl phenanthrolines: synthesis and photophysical and electrochemical characterization, *Polyhedron* 95 (2015) 14–23.
- [56] T. Vadivel, M. Dhamodaran, S. Kulathoaran, S. Kavitha, K. Amirthaganesan, S. Chandrasekaran, S. Ilayaraja, S. Senguttuvan, Rhodium(III) complexes derived from complexation of metal with azomethine linkage of chitosan biopolymer Schiff base ligand: spectral, thermal, morphological and electrochemical studies, *Carbohydr. Res.* 487 (2020) 107878.
- [57] H. Türkmen, T. Pape, F.E. Hahn, B. Cetinkaya, Efficient transfer hydrogenation using iridium and rhodium complexes of benzannulated N-heterocyclic carbenes, *Eur. J. Inorg. Chem.* 5418–5423 (2008).
- [58] M. Ramesh, G. Venkatachalam, Half-sandwich (η^6 -p-cymene) ruthenium(II) complexes bearing 5-amino-1-methyl-3-phenylpyrazole Schiff base ligands: synthesis, structure and catalytic transfer hydrogenation of ketones, *J. Organomet. Chem.* 880 (2019) 47–55.
- [59] V.R. Landaeta, A.D. Salazar-La Rosa, R.E. Rodriguez-Lugo, Transfer hydrogenation of ketones catalyzed by iridium-bulky phosphine complexes, *Inorg. Chim. Acta* 470 (2018) 303–311.
- [60] N.B. Jokić, M. Zhang-Prese, S.L.M. Goh, C.S. Straubinger, B. Bechlars, W. A. Herrmann, F.E. Kühn, Symmetrically bridged bis-N-heterocyclic carbene rhodium (I) complexes and their catalytic application for transfer hydrogenation reaction, *J. Organomet. Chem.* 696 (2011) 3900–3905.
- [61] D.E. Karakaş, F. Durap, A. Baysal, Y.S. Ocak, K. Rafikova, E.Ç. Kaya, A. Zazybin, H. Temel, C. Kayan, N. Meriç, M. Aydemir, Transfer hydrogenation reaction using novel ionic liquid based Rh(I) and Ir(III)-phosphinite complexes as catalyst, *J. Organomet. Chem.* 824 (2016) 25–32.